PHYSICAL REVIEW B **79**, 214420 (2009)

# Coupled structural/magnetocrystalline anisotropy transitions in the doped perovskite cobaltite $Pr_{1-x}Sr_xCoO_3$

C. Leighton,[1,*] D. D. Stauffer,[1] Q. Huang,[2] Y. Ren,[3] S. El-Khatib,[1,2] M. A. Torija,[1] J. Wu,[1] J. W. Lynn,[2] L. Wang,[1] N. A. Frey,[4] H. Srikanth,[4] J. E. Davies,[5] Kai Liu,[5] and J. F. Mitchell[6]

[1]*Department of Chemical Engineering and Materials Science, University of Minnesota, Minneapolis, Minnesota 55455, USA*

[2]*NIST Center for Neutron Research, National Institute of Standards and Technology, Gaithersburg, Maryland 20899, USA*

[3]*Advanced Photon Source, Argonne National Laboratory, Argonne, Illinois 60439, USA*

[4]*Department of Physics, University of South Florida, Tampa, Florida 33620, USA*

[5]*Department of Physics, University of California, Davis, California 95616, USA*

[6]*Materials Science Division, Argonne National Laboratory, Argonne, Illinois 60439, USA*

(Received 24 March 2009; revised manuscript received 24 May 2009; published 15 June 2009)

Years of intensive work on perovskite manganites has led to a detailed understanding of the phenomena that emerge from competition between the electronic and lattice degrees of freedom in these correlated electron systems. It is well understood that the related cobaltites provide an additional spin-state degree of freedom. Here, we use the magnetic properties of a particular cobaltite, $Pr_{1-x}Sr_xCoO_3$, to demonstrate the vital role played by a further ingredient often negligible in manganites; magnetocrystalline anisotropy. $Pr_{1-x}Sr_xCoO_3$ exhibits an anomalous "double magnetic transition" that cannot be ascribed to a spin-state transition or the usual charge/orbital/antiferromagnetic ordering and has thus far evaded explanation. We show that this is actually due to a coupled structural/magnetocrystalline anisotropy transition driven, in this case, by Pr-O hybridization. The results point to the existence of a distinct class of phenomena in the cobaltites due to the unique interplay between structure and magnetic anisotropy.

DOI: 10.1103/PhysRevB.79.214420 PACS number(s): 75.25.+z, 75.30.Gw, 75.47.Gk

The multifunctional nature of complex oxides such as perovskites provides great opportunities for basic science as well as considerable application potential in oxide electronics. The fascinating magnetism of the manganites is a good example. The interplay between charge, spin, lattice, and orbital degrees of freedom[1,2] results in close competition between multiple ground states, leading to such phenomena as magnetoelectronic phase separation[3,4] and colossal magnetoresistance (MR).[1–4] At the same time, high spin polarization,[5–7] interface stability with other oxides, and multiferroicity[8–10] offer exciting opportunities for device function. The Co-based sister compounds of the manganites have been less intensively studied. It is known that the similar Hund's rule exchange and crystal-field energies lead to an additional spin-state degree of freedom in the cobaltites [e.g., $LaCoO_3$ (Ref. 11–16)] but their significant magnetocrystalline anisotropy (MCA) has not been so extensively discussed. Both for basic science and potential applications, the presence of MCA is important. The use of anisotropy, whether it be intrinsic, surface, interface, or exchange induced, is one of the most useful strategies for control of the magnetic response of structures based on conventional ferromagnetic (F) metals[17] but is an aspect that is missing in manganites, which are often essentially isotropic Fs.[2,18–21]

In this paper the presence and importance of MCA in the cobaltites and the role it plays in generating physical phenomena not possible in other systems is illustrated via the unusual properties of $Pr_{1-x}Sr_xCoO_3$ (PSCO). At half doping, multiple studies have found PSCO to exhibit anomalous magnetic properties not present in other $Ln_{1-x}AE_xCoO_3$ (Ln=lanthanide and AE=alkaline-earth) systems.[22–28] Although the typical paramagnet (P) to F transition is found at a Curie temperature ($T_C$) of 230 K (similar to other moderate-to-large bandwidth cobaltites[29]), it is followed, at 120 K, by a second magnetic transition with apparently paradoxical character.[22–28] The magnetization ($M$) decreases, increases (by a factor of 2), or shows no anomaly on cooling, depending on the applied magnetic field. Any signature of this transition in electronic transport is surprisingly absent.[22–25] Many explanations have been conjectured, mostly based on the factors commonly at play in manganites and other cobaltites (e.g., charge/orbital/antiferromagnetic (AF) ordering, spin-state transitions, ferrimagnetism, etc.[22–28]) but there has been no definitive explanation. We show here that the observed transition is actually a coupled structural/MCA transition that naturally explains all aspects of the physical behavior of this material.

Bulk polycrystals ($0.00<x<0.70$) were prepared by solid-state reaction in air. Stoichiometric quantities of $Pr_2O_3$, $SrCO_3$, and $Co_3O_4$ powders were reacted at 1000 °C for 7 days with several intermediate grindings followed by cold pressing, sintering at 1200 °C for 1 day, and slow cooling to room temperature (1 °C/min). Oxygen content was determined by thermogravimetric analysis. In common with other cobaltites, such as $La_{1-x}Sr_xCoO_3$, oxygenation becomes increasingly difficult at higher $x$, particularly above $x=0.5$. The oxygen deficiency ($\delta$ in $Pr_{1-x}Sr_xCoO_{3-\delta}$) was found to increase slowly from 0.07 to 0.12 as $x$ increased from 0.20 to 0.50. Note that the temperature of the magnetic anomaly discussed in this paper is uncorrelated with the doping dependence of the oxygen content (there are approximately 0.1 missing oxygen atoms per unit cell across the whole doping range) and that this magnetic anomaly is unaffected by high-pressure oxygen annealing, which is strong evidence that the effect is not intrinsically related to oxygen vacancies. Magnetometry was performed in a commercial superconducting

 

quantum interference device magnetometer under the conditions described in the text. The transport measurements were performed using a 13.7 Hz a.c. (alternating current) excitation with In contacts in a van der Pauw configuration while a commercial system was employed for heat-capacity measurements via the relaxation method. High-resolution high-energy x-ray powder diffraction (XPD) was performed at beamline 11-ID-C of the advanced photon source (wavelength, $\lambda=0.108$ Å). Neutron powder diffraction (NPD) was done on the BT-1 instrument at the NIST Center for Neutron Research (NCNR), using $\lambda=1.5403$ Å from a Cu(311) monochromator. Collimators with horizontal divergences of 15′, 20′, and 7′ of arc were used before and after the monochromator and after the sample, respectively. Additional diffraction and magnetic order-parameter data were obtained on the BT-2 triple axis spectrometer using a pyrolytic graphite PG(002) monochromator and filter at $\lambda=2.359$ Å. Small-angle neutron scattering (SANS) employed the NG7 instrument at the NCNR and was performed in the scattering wave-vector range $0.01<q<0.3$ Å$^{-1}$. Structural refinements used the general structure analysis system (Ref. 30) with neutron-scattering amplitudes of 0.445, 0.702, 0.253, and 0.581 ($\times 10^{-12}$ cm) for Pr, Sr, Co, and O, respectively. The first-order reversal curve (FORC) method was used to extract the fraction of magnetization that switches irreversibly, as described elsewhere.[31] Finally, direct measurements of the anisotropy field were made via transverse susceptibility measurements performed using a radio frequency (12 MHz) tunnel diode oscillator technique. This method has been validated as a probe of magnetic anisotropy in earlier work.[32] The data were analyzed under the assumption of uniaxial anisotropy, enabling extraction of an effective anisotropy field, $H_k$.

The macroscopic magnetic properties of $Pr_{0.5}Sr_{0.5}CoO_3$ that have drawn such attention are shown in Figs. 1(c) and 1(g)–1(i) for bulk polycrystals. As shown in Fig. 1(c) the material undergoes a F to P phase transition around 230 K. The large splitting between field cooled (FC) and zero-field cooled (ZFC) $M(T)$ is due to the applied field ($\mu_0 H=1$ mT) being much lower than the coercive field, $H_C$,[33] similar to other doped cobaltites,[29] where the MCA is significant.[29,33–36] The dramatic difference in comparison to other systems is the behavior near 120 K where a sharp decrease in $M(T)$ occurs, accompanied by thermal hysteresis. Clearly a magnetic transition occurs at this temperature, which has been dubbed $T_A$ in prior work.[25] The anomalous nature of this transition becomes more apparent when one considers the $H$ dependence of $M(T)$ shown in Figs. 1(g)–1(i). At $\mu_0 H=1$ mT the transition results in a sharp decrease in $M$ on cooling below 120 K while for $\mu_0 H=0.1$ T a sharp *increase* in $M$ occurs on cooling. The crossover field delineating these two regimes is around 75 mT. If the measurement is repeated in a saturating field [$\mu_0 H=5$ T, Fig. 1(i)] no anomaly occurs at $T_A$.

Some of the most obvious potential explanations include charge/orbital/AF ordering, which occur in the equivalent doped manganite[1–4] and a spin-state transition, which is common in cobaltites.[11–16] In both of these cases a clear signature in resistivity ($\rho$) is expected, driven by the charge ordering in the former case and the change in orbital occupancy in the latter. The data of Figs. 2(a) and 2(b) demonstrate that anomalies in $\rho(T)$ near 120 K are notably absent; no anomalies occur at any $x$ value between 0.0 and 0.70 [Fig. 2(a)]. For $x=0.50$ [Fig. 2(b)] $\rho(T)$ shows a change in slope at $T_C$ but no feature at 120 K. The 9 T MR [Fig. 2(c)] shows no anomaly at 120 K either, just a peak near $T_C$.[29] This apparent decoupling of magnetization and transport is unusual in perovskites where the double exchange mechanism provides an inextricable link between $e_g$ electron hopping and F spin alignment.[1–4] The heat-capacity ($C_p$) data [Fig. 2(d)] reveal interesting features however. The usual field-dependent anomaly is observed at $T_C$, in addition to a small *field-independent* kink at $T_A$.

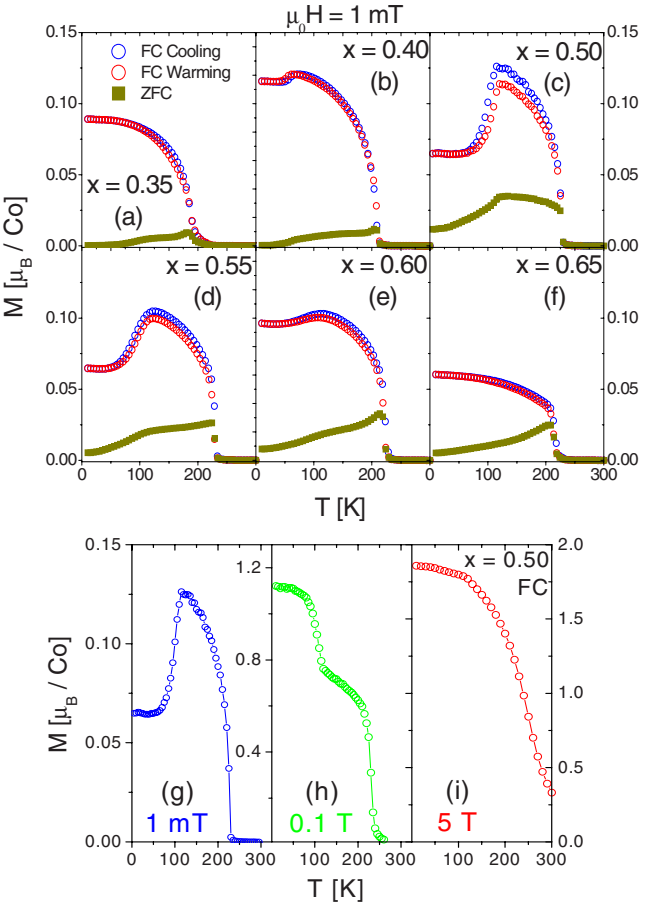


FIG. 1. (Color online) Temperature dependence of the magnetization of $Pr_{1-x}Sr_xCoO_3$. (a)–(f) show 1 mT field cooled (both warming and cooling) and zero-field-cooled data at $x=0.35$, 0.40, 0.50, 0.55, 0.60, and 0.65 in a measuring field of 1 mT. (g)–(i) show the $x=0.5$ field-cooled data at measuring fields of 1 mT, 0.1 T, and 5 T.

The study of the magnetic properties was expanded to multiple $x$ values ($0.0<x<0.70$) in order to better understand the global behavior. $M(T)$ curves for six representative samples are shown in Figs. 1(a)–1(f), at $\mu_0 H=1$ mT. Clearly, the anomalous transition is most prevalent around $x=0.50$. At $x=0.35$ the system is already in an F metallic ground state with a 200 K $T_C$ but no anomaly is found at lower $T$. As $x$ increases to 0.40 the anomaly is first detected as a weak perturbation in $M$ at $T_A=75$ K, increasing to a large change at $T_A=120$ K for $x=0.50$, then vanishing again

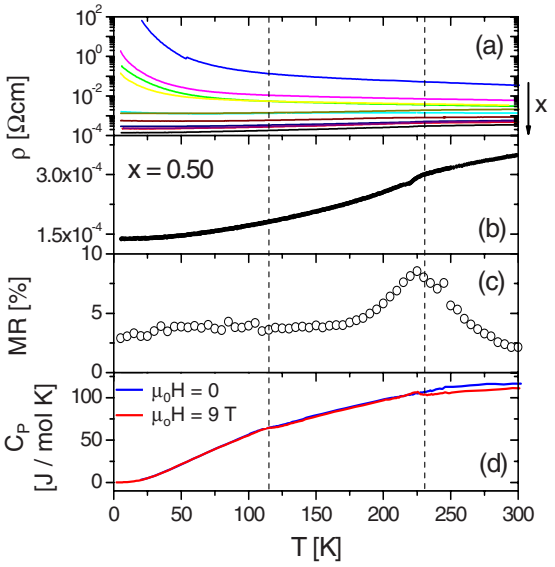


FIG. 2. (Color online) Temperature dependence of the electronic transport and thermodynamic properties. (a) shows the resistivity at $x=0.10$, 0.15, 0.18, 0.20, 0.25, 0.35, 0.40, 0.45, 0.50, 0.55, and 0.60. The resistivity for $x=50$ is shown more clearly in (b) along with the corresponding 9 T magnetoresistance in (c). Specific heat is displayed in (d) both in zero field and 9 T. The vertical dotted lines denote $T_C$ and $T_A$.

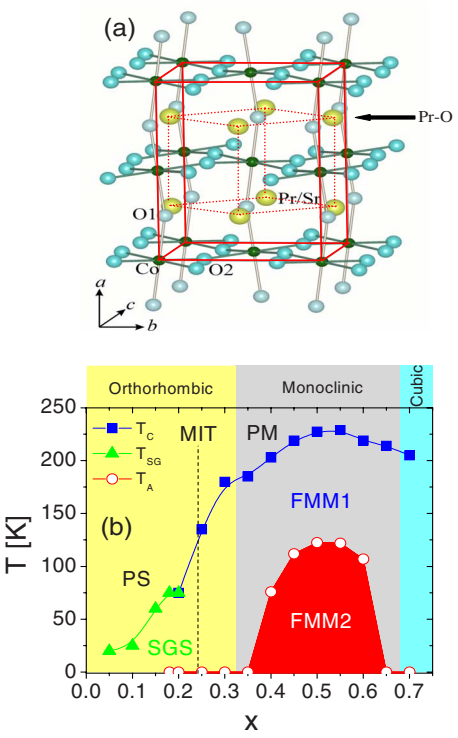


FIG. 3. (Color online) Crystal structure and phase diagram. (a) Crystal structure of $Pr_{0.5}Sr_{0.5}CoO_3$ with monoclinic (solid lines) and pseudocubic (doted lines) unit cells highlighted. The arrow indicates the Pr-O plane discussed in the text. (b) Magnetic phase diagram showing $T_C$, $T_{SG}$, and $T_A$. PS=paramagnetic semiconductor, SGS=spin/cluster-glass semiconductor, PM=paramagnetic metal, FMM=ferromagnetic metal, and MIT=metal-insulator transition. The shaded fields indicate the regions in which the *low T* crystal structure is orthorhombic, monoclinic, and simple cubic.

for $x>0.60$. These results, when combined with a.c. susceptibility (not shown) result in the phase diagram of Fig. 3(b). Similar to the other doped perovskite cobaltites (e.g., $La_{1-x}Sr_xCoO_3$), the system evolves from a spin/cluster glass at low $x$ (due to formation of hole-rich F clusters in a non-F matrix[29,37–39]) to a F metal beyond $x\approx0.20$. This critical doping is the point at which the clusters coalesce, leading to long-range F order and a coincident percolation transition.[29,38,39] The most notable feature is clearly the dome (labeled FMM2) formed by $T_A(x)$, which bounds the region of anomalous magnetism.

High-resolution synchrotron XPD and NPD was performed at $x=0.50$ to determine the crystal structure and probe a possible structural change at $T_A$. In agreement with recent studies,[27,28,40] we refined the structure as monoclinic (space group $I2/a$) at *all* temperatures (3.5 K$<T<$300 K).[41] As a representative example, the standard parameters used to assess the agreement between the structural model and the observed pattern (i.e., the residuals and $\chi^2$ values) are $R_p=4.59\%$, $R_{wp}=5.86\%$, and $\chi^2=1.493$ for the NPD data at 3.5 K. The structure is illustrated in Fig. 3(a). The most important feature is the behavior in the vicinity of 120 K which is shown in Fig. 4(a) for the illustrative case of the region near the (022) and (400) reflections. A dramatic transition occurs near 120 K where the crystal symmetry remains unaltered but the lattice parameters undergo a large change. Such a feature was alluded to in prior work[26] and has been observed with coarse (150 K, cf. 80 K) $T$ resolution.[27] The lattice parameters are plotted in Fig. 4(b) where it can be seen that $a$ and $b$ undergo large changes (+1.15 and −1.10%, respectively) on cooling, the volume of the unit cell being barely affected. Given the similar temperatures for the magnetic and structural transitions we presume the two are related. We also performed a similar XPD study at $x=0.30$, where $T_A=0$ [see Figs. 1(a) and 3(b)], i.e., no such anomalous magnetic transition is present. The structure was refined as orthorhombic at all $T$ with no $T$-dependent transition in lattice parameters. Our structure determinations are consistent with prior work concluding that $Pr_{1-x}Sr_xCoO_3$ is orthorhombic to $x=0.30$ (Ref. 40) and monoclinic to $x=0.67$ (Ref. 42) to 0.80 (Refs. 40 and 43) beyond which fully oxygenated specimens are simple cubic.

NPD was also performed to determine the influence of this lattice anomaly on magnetic ordering. Figure 4(c) shows the $T$ dependence of the NPD intensity around (011) and (200) peaks [complementary to Fig. 4(a)]. The limited resolution results in a single peak at $T>120$ K, which broadens below 120 K due to the increased splitting between (200) and (011). $T_C$ is observed as an onset of additional intensity near 230 K, followed at 120 K by a sharp decrease in the maximum intensity [upper panel of Fig. 4(d)], apparently suggesting a discontinuity in order parameter. Such a perfunctory analysis belies the true physics, as both overlapping reflections [(200) and (011)] possess significant magnetic intensity. To account for this we performed a two-Gaussian fitting procedure to extract the individual intensities. [The positions of the two peaks are shown as dotted lines in Fig. 4(c). Note that at low temperatures it is clear from the peak

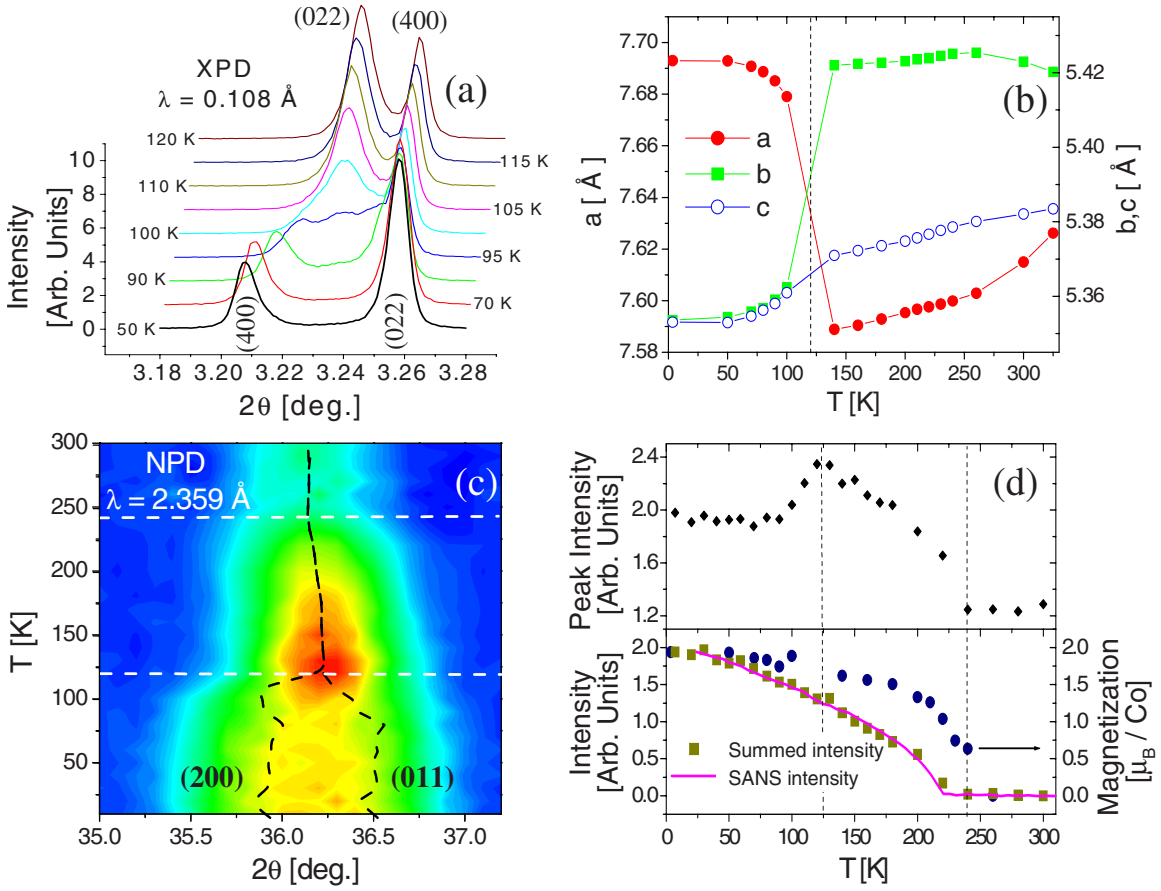


FIG. 4. (Color online) X-ray and neutron scattering results ($x$=0.5). Panel (a) shows the temperature dependence of the x-ray diffraction patterns in the vicinity of the (400) and (022) peaks. The lattice parameters determined from the x-ray diffraction are shown in (b). Panel (c) is a (color) intensity plot showing the intensity of the neutron diffraction near the (011) and (200) peaks. The dotted lines depict the individual diffraction peaks as discussed in the text. The peak neutron intensity vs temperature is shown in the top panel of (d), along with the refined saturation moment (right axis), small-angle neutron-scattering intensity ($q$=0.0138 Å$^{-1}$), and the "summed intensity" described in the text (left axis). The dotted lines denote $T_C$ and $T_A$.

profile that two overlapping reflections clearly exist and can be reliably separated.] When these intensities are summed [$(I_{011}+I_{200})$ vs $T$, Fig. 4(d), solid squares] one observes no anomaly at all in the magnetic order parameter. The magnetic moment extracted from full refinements (which is independent of this two-Gaussian fitting procedure) is also plotted in Fig. 4(d), again showing no feature at 120 K. These refinements indicate no detectable ordering of Pr moments or changes in the symmetry of magnetic ordering at $T_A$. We also measured SANS from a sintered polycrystal. The magnetic SANS intensity at $q$=0.014 Å$^{-1}$ (which is due to domains and domain walls and scales with the magnetization[44]) is shown as the solid line in Fig. 4(d), again confirming the absence of an anomaly in order parameter at 120 K. These data rule out several plausible explanations. There is no evidence of AF phase formation, ordering of the Ln moments [which could lead to ferrimagnetism if AF coupled to the Co spin sublattice as in $Nd_{1-x}Sr_xCoO_3$ (Ref. 35)], or any discontinuity in the F order parameter. This is, however, completely consistent with the absence of anomalies in $\rho(T)$, MR($T$), and $M_S(T)$.

Having ruled out charge/orbital ordering, spin-state transitions, AF ordering, and ferrimagnetism, and given the absence of any transition in magnetic order parameter, the natural conclusion is that the structural transition at 120 K leads only to changes in the low-field magnetization [Figs. 1(g) and 1(h)], not the saturated moment [Fig. 1(i)]. The MCA, which has a strong influence on the domain distribution and magnetization reversal mechanisms, in turn controlling coercivity and remanence, is one possible source. In order to probe this possibility we measured the $T$ dependence of (a) the coercivity ($H_C$) and remanence (from isothermal major hysteresis loops), (b) the fraction of magnetization that switches irreversibly (from first-order reversal curves), and (c) the effective anisotropy field ($H_K$) (from transverse susceptibility), as shown in Figs. 5(a)–5(c). As pointed out by Mahendiran and Schiffer[25] $H_C$ does indeed show an anomaly at 120 K. This takes the form of a sharp decrease in $H_C$ on cooling through $T_A$, accompanied by an abrupt decrease in remanent magnetization (data not shown), strong evidence of a discontinuous decrease in anisotropy constant on cooling. Figure 5(b) shows that the fraction of $M$ that switches irreversibly is also consistent with such an interpretation. Finally, the $H_K(T)$ data of Fig. 5(c) provide unequivocal evidence for a transition from a high $T$ higher MCA region to a low $T$ lower MCA region, the anisotropy field falling by

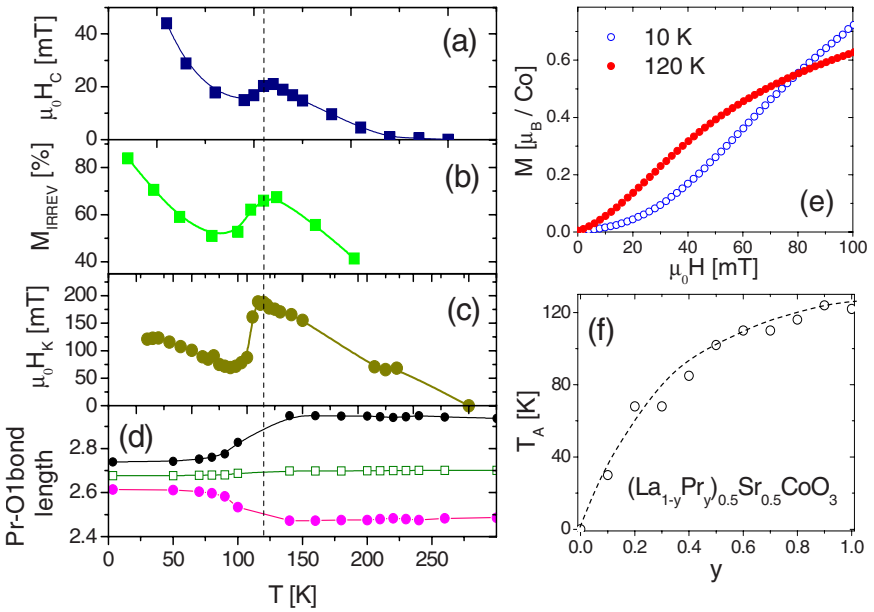


FIG. 5. (Color online) The magnetic anisotropy transition in $Pr_{0.5}Sr_{0.5}CoO_3$. (a)–(d) show the temperature dependence of the coercivity ($H_C$), fraction of irreversible magnetization ($M_{IRREV}$), anisotropy field ($H_K$), and Pr-O1 bond lengths [see structure in Fig. 3(a)]. The dotted line denotes $T_A$. Panel (e) shows the field dependence of the magnetization at illustrative temperatures of 10 and 120 K. Panel (f) displays the $y$ dependence of $T_A$ in $(La_{1-y}Pr_y)_{0.5}Sr_{0.5}CoO_3$.

about a factor of 3 between 120 and 80 K. The 10 K $H_K$ values from Fig. 5(c) correspond to uniaxial anisotropy constants in the mid $10^5$ erg/cm$^3$ range, roughly consistent with prior estimates in $La_{1-x}Sr_xCoO_3$.[36]

The coupled lattice-MCA transition implicated by these data provide a simple explanation for the puzzling data of Figs. 1(g) and 1(h). The complex field dependent $M(T)$ on cooling through $T_A$ is due to the changes in the (MCA-dependent) parameters describing the hysteresis loop shape ($H_C$, remanence, field-dependent susceptibility, etc.) when $H<H_S$ (the saturation field). A simple illustration of how this can lead to either a decrease or increase in $M$ as $T$ is lowered through $T_A$ is provided in Fig. 5(e) showing magnetizing $M(H)$ curves after zero-field cooling to 10 ($T \ll T_A$) and 120 K ($T \approx T_A$). The 10 K curve exhibits a faster approach to saturation than the 120 K curve at high fields (consistent with the lower MCA) but has a *smaller* initial susceptibility, leading to a crossing of the two curves around 75 mT. The result is that at $\mu_0 H < 75$ mT $M$ increases with $T$ from 10 to 120 K while at 75 mT $< \mu_0 H < \mu_0 H_S$, $M$ decreases with $T$ from 10 to 120 K, providing a simple explanation for the data of Figs. 1(g)–1(i). The smaller initial susceptibility in the lower MCA region can be explained by poor magnetic coupling between grains at low $T$. This proposed structural-MCA transition also explains all other observed phenomena. The absence of a transition in $\rho(T)$ and MR($T$) is natural given the unaffected magnetic order parameter. The anomaly in $C_p(T)$ at 120 K is due to the structural transition while it's field independence indicates the absence of any change in spin entropy, consistent with a transition in the MCA rather than the magnetic moment.

These results demonstrate a transition in the *magnitude* of the anisotropy constant during the structural transition at $T_A$. A change in the *direction* of the magnetic easy axis also occurs. Examining the recently published Lorentz microscopy images of Uchida *et al.*[26] in tandem with the results of our structural studies enable us to further understand this. This magnetically sensitive microscopy reveals band-type magnetic domains whose magnetization reorients between [110] and [100] at a temperature between 140 and 80 K, i.e., a rotation of the easy axis of magnetization occurs near $T_A$.[45] Similarly, Hirahara *et al.*[28] observed a transition to a [100] easy axis at low temperatures using conventional magnetometry on single crystals. This reorientation of the magnetic easy axis is clearly driven by the transition in $a$- and $b$-axis lattice parameters (i.e., an $a$-$b$ plane rearrangement) shown in Fig. 4(b). The extended $a$-axis lattice parameter below $T_A$ results in a much larger difference between Co-O1 and Co-O2 bond lengths as well as a transition from the Co-O2-Co bond angle being closer to 180° to the Co-O1-Co angle being closer to 180°, both factors playing an important role in determining the easy axis. We speculate that a suitably sophisticated electronic structure calculation could quantitatively reproduce the change in MCA magnitude and direction given the experimentally determined changes in structure. As a final remark on this issue, it is worth pointing out that what we observe here is not simply a spin reorientation transition in the conventional sense, i.e., a transition driven by competing anisotropies. In our case the change occurs in both the magnitude of the anisotropy constant and the direction of easy axis of the magnetization, and, crucially, is driven by a simultaneous structural phase transition.

The final issue is the *origin* of this structural transition. The absence of such a transition in other $Ln_{0.5}AE_{0.5}CoO_3$ cobaltites [Ln=La, Nd, Gd, Sm, or Eu, and AE=Sr, Ca, or Ba (Refs. 11, 22–24, 29, and 33–39)] implies some involvement of the Pr ion itself. In agreement with Troyanchuk *et al.*[27] we hypothesize that the unusual tendency of Pr 4$f$ orbitals to hybridize with O 2$p$ orbitals[27,46] leads to Pr playing an active role in the $Pr_{1-x}Sr_xCoO_3$ bonding. This hybridization effect is in fact well known in high-temperature superconductivity and is responsible for the fact that $PrBa_2Cu_3O_{7-\delta}$ is the *only* nonsuperconducting member of the $LnBa_2Cu_3O_{7-\delta}$ family.[46] Our hypothesis was tested via measurement of the magnetic transition temperature, $T_A$, at 11 compositions in the $(La_{1-y}Pr_y)_{0.5}Sr_{0.5}CoO_3$ series. The results [Fig. 5(f)] are remarkable; $T_A$ is found to increase from zero at $y=0$, reaching 30 K already by $y=0.10$, eventually satu-

rating at 120 K at $y=1.0$, i.e., the data confirm that the presence of even small Pr concentrations leads to onset of the effect. The important role played by Pr-O bonding in PSCO is further evidenced by the $T$ dependence of the Pr-O bond lengths [Fig. 5(d)]. At $T>T_A$ the three inequivalent Pr-O1 bond lengths in the monoclinic Pr-O planes [see Fig. 3(a)] differ by as much as 0.4 Å. The situation changes dramatically on cooling. Although the intermediate Pr-O1 bond length remains approximately constant, the largest bond length undergoes a large decrease (7.1%) and the smallest undergoes a large increase (5.7%). In essence, there is a strong tendency to equalize the three inequivalent Pr-O1 bond lengths below $T_A$, consistent with the concept that Pr-O bonding plays an active role in dictating the crystal structure rather than simply adapting to the structure dictated by the bonding in the network of corner-sharing Co-O octahedra. The transition at $T_A$ thus arises due to competition between the Pr-O covalent bonding (which drives equalization of the Pr-O1 bond lengths) and the usual cooperative distortion of the Co-O octahedra required to accommodate tolerance factors less than 1 (which necessarily requires disparate Pr-O1 bond lengths). Such a picture also provides an explanation for the localization of this transition to $0.35<x<0.65$ [Fig. 3(b)]. The key point is that PSCO has been observed to be orthorhombic for $x\leq 0.30$ (Ref. 40) (consistent with this work) and simple cubic at $x=0.67$ (Ref. 42) and 0.80.[40,43] As shown in Fig. 3(b), the region $0.35<x<0.65$ over which $T_A$ is found to be nonzero thus corresponds to the region of stability of the monoclinic phase, strong evidence that this lower symmetry is essential for this type of structural transition. This is consistent with our argument that initially strongly distinct Pr-O bond lengths are required, as present in the monoclinic structure.

In summary, we have provided a complete explanation for the anomalous magnetic properties of the doped perovskite cobaltite $Pr_{1-x}Sr_xCoO_3$. This is based on the observation of a coupled structural/magnetocrystalline anisotropy transition where a Pr-O hybridization-driven change in lattice parameters results in a sharp change in both the magnitude of magnetocrystalline anisotropy and direction of easy axis of magnetization. This picture provides a consistent explanation for all phenomena including the field and temperature dependence of the magnetization, the absence of transport anomalies, the behavior of the specific heat, and the doping dependence of the transition. Our results emphasize the dominant role played by magnetocrystalline anisotropy in the cobaltites and constitute the first step in unraveling the physics that arises from the general interplay between magnetic anisotropy and structure in these materials.

Work was supported primarily by DOE (Grant No. DE-FG02-06ER46275) and in part by NSF (Grant No. DMR-0804432), and U.S. Department of Commerce. Work at USF was supported by DOE (Grant No. DE-FG02-07ER46438) Work at UCD was supported by CITRIS. Use of the Advanced Photon Source at ANL was supported by the DOE (Grant No. DE-AC02-06CH11357).

*Author to whom correspondence should be addressed; leighton@umn.edu

[1] Y. Tokura and Y. Tomioka, J. Magn. Magn. Mater. **200**, 1 (1999).
[2] J. M. D. Coey, M. Viret, and S. von Molnár, Adv. Phys. **48**, 167 (1999).
[3] E. Dagotto, *Nanoscale Phase Separation and Colossal Magnetoresistance* (Springer, New York, 2002).
[4] E. Dagotto, T. Hotta, and A. Moreo, Phys. Rep. **344**, 1 (2001).
[5] Y. Ji, C. L. Chien, Y. Tomioka, and Y. Tokura, Phys. Rev. B **66**, 012410 (2002).
[6] B. Nadgorny, I. I. Mazin, M. Osofsky, R. J. Soulen, P. Broussard, R. M. Stroud, D. J. Singh, V. G. Harris, A. Arsenov, and Ya. Mukovskii, Phys. Rev. B **63**, 184433 (2001).
[7] M. Bowen, M. Bibes, A. Barthelemy, J.-P. Contour, A. Anane, Y. Lemaitre, and A. Fert, Appl. Phys. Lett. **82**, 233 (2003).
[8] S. W. Cheong and M. Mostovoy, Nature Mater. **6**, 13 (2007).
[9] D. I. Khomskii, J. Magn. Magn. Mater. **306**, 1 (2006).
[10] R. Ramesh and N. A. Spaldin, Nature Mater. **6**, 21 (2007).
[11] J. B. Goodenough and J. S. Zhou, in *Structure and Bonding*, edited by J. B. Goodenough (Springer, New York, 2001), pp. 17–113.
[12] K. Asai, O. Yokokura, N. Nishimori, H. Chou, J. M. Tranquada, G. Shirane, S. Higuchi, Y. Okajima, and K. Kohn, Phys. Rev. B **50**, 3025 (1994).
[13] A. Podlesnyak, S. Streule, J. Mesot, M. Medarde, E. Pomjakushina, K. Conder, A. Tanaka, M. W. Haverkort, and D. I. Khomskii, Phys. Rev. Lett. **97**, 247208 (2006).
[14] M. W. Haverkort, Z. Hu, J. C. Cezar, T. Burnus, H. Hartmann, M. Reuther, C. Zobel, T. Lorenz, A. Tanaka, N. B. Brookes, H. H. Hsieh, H. J. Lin, C. T. Chen, and L. H. Tjeng, Phys. Rev. Lett. **97**, 176405 (2006).
[15] D. P. Kozlenko, N. O. Golosova, Z. Jirak, L. S. Dubrovinsky, B. N. Savenko, M. G. Tucker, Y. Le Godec, and V. P. Glazkov, Phys. Rev. B **75**, 064422 (2007).
[16] R. F. Klie, J. C. Zheng, Y. Zhu, M. Varela, J. Wu, and C. Leighton, Phys. Rev. Lett. **99**, 047203 (2007).
[17] J. B. Kortright, D. D. Awschalom, J. Stohr, S. D. Bader, Y. U. Idzerda, S. S. P. Parkin, I. K. Schuller, and H.-C. Siegmann, J. Magn. Magn. Mater. **207**, 7 (1999).
[18] M. B. Salamon and M. Jaime, Rev. Mod. Phys. **73**, 583 (2001).
[19] J. W. Lynn, R. W. Erwin, J. A. Borchers, Q. Huang, A. Santoro, J.-L. Peng, and Z. Y. Li, Phys. Rev. Lett. **76**, 4046 (1996).
[20] J. A. Fernandez-Baca, P. Dai, H. Y. Hwang, C. Kloc, and S. W. Cheong, Phys. Rev. Lett. **80**, 4012 (1998).
[21] Orbital-order-induced anisotropy may be an exception to this general statement. See, for example, S. Cao, B. Kang, J. Zhang, and S. Yuan, Appl. Phys. Lett. **88**, 172503 (2006).
[22] K. Yoshii, A. Nakamura, H. Abe, M. Mizumaki, and T. Muro, J. Magn. Magn. Mater. **239**, 85 (2002).
[23] H. Masuda, T. Fujita, T. Miyashita, M. Soda, Y. Yasui, Y. Kobayashi, and M. Sato, J. Phys. Soc. Jpn. **72**, 873 (2003).

[24] K. Yoshii and H. Abe, Phys. Rev. B **67**, 094408 (2003).
[25] R. Mahendiran and P. Schiffer, Phys. Rev. B **68**, 024427 (2003).
[26] M. Uchida, R. Mahendiran, Y. Tomioka, Y. Matsui, K. Ishizuka, and Y. Tokura, Appl. Phys. Lett. **86**, 131913 (2005).
[27] I. O. Troyanchuk, D. V. Karpinskii, A. N. Chobot, D. G. Voitsekhovich, and V. M. Bobryanskii, JETP Lett. **84**, 151 (2006).
[28] S. Hirahara, Y. Nakai, K. Miyoshi, K. Fujiwara, and J. Takeuchi, J. Magn. Magn. Mater. **310**, 1866 (2007).
[29] J. Wu and C. Leighton, Phys. Rev. B **67**, 174408 (2003).
[30] A. C. Larson and R. B. Von Dreele, Los Alamos National Laboratory Report No. LAUR086–748, 1990 (unpublished).
[31] J. E. Davies, J. Wu, C. Leighton, and K. Liu, Phys. Rev. B **72**, 134419 (2005).
[32] G. T. Woods, P. Poddar, H. Srikanth, and Y. M. Mukovskii, J. Appl. Phys. **97** 10C104 (2005).
[33] P. S. Anil Kumar, P. A. Joy, and S. K. Date, J. Phys.: Condens. Matter **10**, L487 (1998).
[34] A. Senchuk, H. P. Kunkel, R. M. Roshko, C. Viddal, L. Wei, G. Williams, and X. Z. Zhou, Eur. Phys. J. B **37**, 285 (2004).
[35] D. D. Stauffer and C. Leighton, Phys. Rev. B **70**, 214414 (2004).
[36] H. M. Aarbogh, J. Wu, L. Wang, H. Zheng, J. F. Mitchell, and C. Leighton, Phys. Rev. B **74**, 134408 (2006).
[37] P. L. Kuhns, M. J. R. Hoch, W. G. Moulton, A. P. Reyes, J. Wu, and C. Leighton, Phys. Rev. Lett. **91**, 127202 (2003).
[38] J. Wu, J. W. Lynn, C. J. Glinka, J. Burley, H. Zheng, J. F. Mitchell, and C. Leighton, Phys. Rev. Lett. **94**, 037201 (2005).
[39] D. Phelan, D. Louca, S. Rosenkranz, S. H. Lee, Y. Qiu, P. J. Chupas, R. Osborn, H. Zheng, J. F. Mitchell, J. R. D. Copley, J. L. Sarrao, and Y. Moritomo, Phys. Rev. Lett. **96**, 027201 (2006).
[40] H. W. Brinks, H. Fjellvag, A. Kjekshus, and B. C. Hauback, J. Solid State Chem. **147**, 464 (1999).
[41] Accurate determination of the monoclinic space group is difficult. In contrast to Refs. 26 and 36 we favor $I2/a$ over $P2_1/n$ based on the absence of reflections with $h+k+l=2n+1$.
[42] M. James, D. Cassidy, D. J. Goossens, and R. L. Withers, J. Solid State Chem. **177**, 1886 (2004).
[43] A. Podlesnyak, A. Mirmelstein, N. Golosova, E. Mithberg, I. Leonidov, V. Kozhevnikov, I. Sashin, F. Altorfer, and A. Furrer, Appl. Phys. A: Mater. Sci. Process. **74**, S1746 (2002).
[44] J. W. Lynn, L. Vasiliu-Doloc, and M. A. Subramanian, Phys. Rev. Lett. **80**, 4582 (1998).
[45] In principle such a rotation can be observed directly from NPD refinements, as claimed in Ref. 27. In our case, significantly higher resolution would be required in order to resolve the (011) and (200) peaks.
[46] M. E. Lopez-Morales, D. Rios-Jara, J. Taguena, R. Escudero, S. La Placa, A. Bezinge, V. Y. Lee, E. M. Engler, and P. M. Grant, Phys. Rev. B **41**, 6655 (1990).